Complete Characterization of an Optical Pulse Based on Temporal Interferometry Using an Unbalanced Temporal Pulse Shaping System

Chao Wang, *Student Member, IEEE, OSA*, and Jianping Yao, *Senior Member, IEEE, Fellow, OSA*

***Abstract*—We propose and demonstrate a simple method for the full characterization of an ultrashort optical pulse based on temporal interferometry, using an unbalanced temporal pulse shaping (UB-TPS) system. The UB-TPS system consists of a Mach–Zehnder modulator and two dispersive elements (DEs) having opposite dispersion, but nonidentical in magnitude. The entire system can be considered as a typical balanced TPS system for a real-time Fourier transformation to generate two time-delayed replicas of the input optical pulse, followed by a residual DE to perform a second real-time Fourier transformation to convert the two time-delayed pulse replicas to two frequency-sheared optical spectra. The spectral interferometry is performed in the time domain. The spectral magnitude and phase information of the input optical pulse is accurately and unambiguously reconstructed from the recorded temporal interference pattern based on a Fourier transform algorithm. Compared with a conventional pulse characterization system based on linear interferometric measurement using an optical interferometer implemented by using discrete components, the proposed system features better stability, higher adaptability, and single-shot measurement. The use of the proposed system for the characterization of a femtosecond pulse before and after passing through a 60-m-long single-mode fiber is experimentally demonstrated.**

***Index Terms*—Chromatic dispersion, pulse characterization, real-time Fourier transform, spectral interferometry, suppressed-carrier (SC) modulation, temporal pulse shaping.**

I. Introduction

ULTRASHORT optical pulses have found wide applications in various scientific and engineering fields [1], such as optical communications, medical diagnostics, and direct observation of ultrafast dynamics. Fast and precise characterization of an optical ultrashort pulse is essential to evaluate and improve the performance of an optical system based on ultrafast optics. An optical pulse used for optical telecommunications typically has a temporal duration ranging from 1 ps to 1 ns. Several approaches for the full characterization (both magnitude and phase) of a picosecond pulse have been recently demonstrated [2], including those based on sonography [3], chronocyclic tomography [4], and spectrography [5]. To fully characterize an optical pulse with a much shorter duration (i.e., a femtosecond pulse), different characterization techniques have been developed in the past few decades [6]. A widely used technique for femtosecond pulse characterization is the frequency-resolved optical gating (FROG) [7] that is implemented based on nonlinear interaction between the probe and the gate pulses. The pulse information is reconstructed from a spectrally resolved cross-correlation profile followed by an iterative phase-retrieval algorithm. A time-domain ultrashort optical pulse characterization method called time-resolved optical gating (TROG) technique has also been proposed [8], in which the gating is performed in the frequency domain by a spectral filter and the cross-correlation trace is temporally resolved by an integrating photodetector (PD). In the cross-correlation-based techniques [7], [8], a known reference pulse is always required. In addition, since the iterative algorithms employed in the aforementioned methods are time-consuming, the pulse characterization cannot be implemented in real time. On the other hand, self-referencing interferometric techniques enabling simple (without a known reference pulse) and direct (noniterative) pulse characterization with higher sensitivity have been recently proposed [9]. For example, spectral phase interferometry for direct electric field reconstruction (SPIDER) [10] is a well-known pulse reconstruction method implemented in the spectral domain based on spectral shearing interferometry [11], where a spectral shear between two replicas of the input optical pulse is generated in a nonlinear material.

Linear self-referencing interferometric measurement can also be done in the time domain based on temporal interferometry [12] where the optical pulse to be characterized is first spectrally dispersed, and then sent to an optical interferometer. The phase of the dispersed pulse can be determined by an optical delay line discriminator. A simple linear transform is then used to retrieve the information of the original pulse. Another application of this technique is the measurement of optical fiber dispersion [13]. A similar time-domain interferometric technique based on real-time spectral interferometry has recently been proposed for the complete characterization of an ultrashort pulse [14], [15]. Unlike the spectral shearing interferometry where the spectral shear is generated in a nonlinear material [10], the frequency shear is obtained by time-shifting two Fourier-transformed waveforms due to the real-time Fourier transformation [16] in a dispersive element. The magnitude and phase information of the original input pulse is reconstructed from the temporal interference of the two stretched and time-delayed pulses,

Manuscript received September 06, 2010; revised January 04, 2011; accepted January 10, 2011. Date of publication January 17, 2011; date of current version March 02, 2011. This work was supported in part by the Natural Sciences and Engineering Research Council of Canada (NSERC).

The authors are with the Microwave Photonics Research Laboratory, School of Information Technology and Engineering, University of Ottawa, ON K1N 6N5, Canada (e-mail: jpyao@site.uottawa.ca).

Color versions of one or more of the figures in this paper are available online at http://ieeexplore.ieee.org.

Digital Object Identifier 10.1109/JLT.2011.2106480

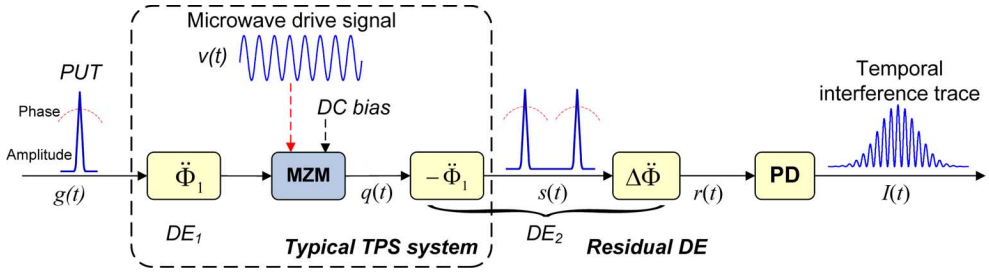

Fig. 1. Schematic of the proposed UB-TPS system that can be modeled as a typical TPS system followed by a residual DE. PUT: pulse under test, DE: dispersive element, TPS: temporal pulse shaping, MZM: Mach–Zehnder modulator, and PD: photodetector.

using the Fourier transform [14], [15] or Hilbert transform [17], [18] algorithms. In the self-referencing time-domain interferometric techniques [12], [14], [15], [17], [18], since the interferogram can be recorded in the time domain by using a high-speed real-time oscilloscope, a complete characterization of an ultrashort optical pulse with a high update rate of up to a gigahertz can be achieved. However, since an optical interferometer implemented by using discrete components, such as a glass plate [14], a fiber-optic Sagnac interferometer [15], or a free-space Michelson interferometer [12], [17], is usually used to generate two time-delayed interfering optical pulses, the performance of pulse characterization methods is greatly affected by the poor stability of the interferometer due to its inherent high sensitivity to environmental perturbations, leading to considerable errors in the phase measurement process. A feedback control loop could be introduced in the interferometer to minimize the measurement errors [18]. However, the whole system becomes complicated, and moreover, the feedback loop can only be updated at a relatively slow rate (usually below 1 MHz) that is not suitable for the characterization of an optical pulse train with a very high update rate.

In this paper, we propose and demonstrate a simple technique for the complete characterization of an ultrashort (subpicosecond) optical pulse based on temporal interferometry without using a discrete optical interferometer. An unbalanced temporal pulse shaping (UB-TPS) system is employed to simultaneously generate and temporally stretch two time-delayed replicas of the input optical pulse to be characterized [19]. It is different from a conventional balanced TPS system [20] where a Mach–Zehnder modulator (MZM) and two dispersive elements (DEs) having exactly complementary dispersion are employed, in the proposed UB-TPS system, the two DEs have opposite dispersion, but nonidentical in magnitude. The proposed UB-TPS system has recently been applied to achieve photonically assisted continuously tunable microwave frequency multiplication [21].

The proposed UB-TPS system is equivalent to a conventional balanced TPS system to perform a real-time Fourier transform for the generation of two time-delayed replicas of the input optical pulse, followed by a residual DE to perform a second real-time Fourier transform for the generation of an equivalent frequency shear. Therefore, the spectral interferometry is performed in the time domain. The spectral magnitude and phase information of the input optical pulse to be measured is retrieved from the recorded temporal interferogram based on the well-known Fourier transform algorithm [22]. The key significance of the proposed technique is that the system stability is greatly improved since the optical interferometer that was implemented by using discrete components in the previous systems is replaced by an MZM that is essentially an integrated waveguide interferometer. It is worth noting that the use of an MZM also enables fast electrical tuning of the time delay between two interfering pulses by controlling the frequency of the microwave modulation signal applied to the MZM, making the technique ideally suitable for practical applications where optical pulses with a variety of repetition rates and pulse durations are to be characterized. This issue will be discussed in more details in Section IV-D.

Some preliminary experimental observations have recently been reported by us [19]. To have a better understanding of the proposed technique, a comprehensive theoretical analysis and further experimental verifications are needed, which are presented in this paper.

The remainder of this paper is organized as follows. In Section II, we first describe the principle of the proposed UB-TPS system in details, with a focus on the generation of two time-delayed pulse replicas in a double-sideband with suppressed carrier (DSB-SC) modulation scheme. Numerical simulations to evaluate the UB-TPS system performance are also performed. In Section III, the principle of optical pulse characterization by using the UB-TPS system is presented. Experimental demonstration of ultrashort optical pulse characterization is also carried out in this section. The full characterization of an optical pulse train with a full-width at half-maximum (FWHM) of ∼810 fs and a repetition rate of 48.6 MHz before and after propagating through a 60-m-long standard single-mode fiber (SMF) is performed. A discussion on the impact of the higher order dispersion on the optical pulse characterization is provided in Section IV. The stability and adaptability of the proposed technique for practical implementations are also presented. A conclusion is drawn in Section V.

II. UB-TPS System

The proposed UB-TPS system is illustrated in Fig. 1. The system consists of an MZM and two DEs having opposite dispersion, but nonidentical in magnitude. The DEs can be two linearly chirped fiber Bragg gratings (LCFBGs) or two dispersive fibers with opposite dispersion.

Here, we assume that the values of the third-order dispersion (TOD) of the two DEs are small and can be ignored, and only the second-order dispersion (SOD) or group velocity dispersion (GVD) is considered in our analysis. This assumption

is usually employed in a temporal-interferometry-based optical pulse characterization system [14]. We also assume that the peak power of the input pulse is low enough to avoid any nonlinear effects in the DEs. Then, the two DEs can then be modeled as linear time-invariant (LTI) systems with transfer functions given by [23]

$$H_i(\omega) = \exp(\frac{-j\ddot{\Phi}_i\omega^2}{2}), \qquad (i = 1, 2) \tag{1}$$

where $\ddot{\Phi}_1$ and $\ddot{\Phi}_2$ (in square picosecond per radian) are the dispersion (GVD) of the two DEs. In the proposed UB-TPS system, the dispersion values should satisfy the conditions $\ddot{\Phi}_1\ddot{\Phi}_2 < 0$ and $|\ddot{\Phi}_1| \neq |\ddot{\Phi}_2|$. The transfer function of the second DE can be rewritten as $H_2(\omega) = \exp(j\ddot{\Phi}_1\omega^2/2)\exp(-j\Delta\ddot{\Phi}\omega^2/2)$, where $\Delta\ddot{\Phi} = \ddot{\Phi}_1 + \ddot{\Phi}_2$ is defined as the residual dispersion. Therefore, the entire UB-TPS system can be modeled as a typical balanced TPS system with a pair of complementary DEs having dispersion of $\ddot{\Phi}_1$ and $-\ddot{\Phi}_1$ [20], followed by a residual DE with a transfer function of $H_\Delta(\omega) = \exp(-j\Delta\ddot{\Phi}\omega^2/2)$, as shown in Fig. 1.

Assume that the microwave drive signal applied to the MZM is a sinusoidal signal given by $V(t) = (\pi/V_\pi) \times V_m \cos(\omega_m t)$, where V_π is the half-wave voltage of the MZM, and V_m and ω_m are the amplitude and angular frequency of the microwave modulation signal, respectively. The intensity modulation function in the MZM can be expressed as [24]

$$\begin{aligned} e_{\mathrm{IM}}(t) &= \frac{1}{2}\left\{\exp\left[i\frac{\phi_0 + V(t)}{2}\right]\right. \\ &\quad \left. + \exp\left[-i\frac{\phi_0 + V(t)}{2}\right]\right\} \\ &= \cos\left[\frac{\phi_0 + V(t)}{2}\right] \end{aligned} \tag{2}$$

where ϕ_0 is a constant phase shift determined by the dc-bias voltage applied to the MZM. Equation (2) can be expanded in Bessel series

$$\begin{aligned} e_{\mathrm{IM}}(t) &= \cos\left[\frac{\phi_0 + V(t)}{2}\right] \\ &= \cos\left(\frac{\phi_0}{2}\right) J_0(\beta) + \sum_{n=1}^{\infty} a_n J_n(\beta)\cos(n\omega_m t) \\ a_n &= \begin{cases} 2 \times \cos\left(\frac{\phi_0}{2}\right) \times (-1)^{n/2}, & \text{n is even} \\ -2 \times \sin\left(\frac{\phi_0}{2}\right) \times (-1)^{(n+1)/2}, & \text{n is odd} \end{cases} \end{aligned} \tag{3}$$

where $J_n(\beta)$ is the Bessel function of the first kind of order n with argument of β, and $\beta = (V_m/V_\pi) \times (\pi/2)$ is the phase modulation index. We can see that the intensity modulation in the MZM would lead to the generation of the first-order and higher order optical sidebands, with the amplitude distribution of these sidebands determined by the variation of the Bessel functions parameterized by β and the constant phase shift ϕ_0.

In our proposed approach, the dc bias voltage of the MZM is tuned to have $\phi_0 = \pi$. This is equivalent that the MZM is dc-biased at the minimum transmission point. Therefore, the optical carrier and all the even-order optical sidebands will vanish, as indicated in (3). In addition, under small-signal modulation condition, all optical sidebands above the second order would have an amplitude that is low enough to be ignored. Therefore, in this DSB-SC modulation scheme, the intensity modulation function can be rewritten as

$$e_{\mathrm{IM}}(t) \cong 2 \times J_1(\beta)\cos\,(\omega_m t) \tag{4}$$

On the other hand, an input pulse under test (PUT) can be expressed as $g(t) = |g(t)|\exp[j\phi(t)]$, with $|g(t)|$ and $\phi(t)$ being the temporal magnitude and phase terms, shown as the solid and dashed lines in Fig. 1, respectively. The PUT is first sent to the first subsystem, the typical balanced TPS system, where it is temporally stretched by the first DE ($\ddot{\Phi}_1$), modulated by the microwave drive signal $V(t)$ at the MZM, and then, completely compressed by a matched DE ($-\ddot{\Phi}_1$), as shown in Fig. 1.

Note that the first DE should have an adequate dispersion to temporally stretch the input optical pulse such that the stretched pulse can be completely modulated by a low-frequency microwave drive signal. It is known that the optical pulse broadening is determined by its spectral bandwidth and the dispersion of the DE [23]. The dispersion of the first DE and modulation frequency must satisfy the following condition:

$$\omega_m > \frac{4\pi}{\tau_0 + \Delta\omega_{\mathrm{opt}} \times \ddot{\Phi}_1} \tag{5}$$

where τ_0 and $\Delta\omega_{\mathrm{opt}}$ are the temporal pulsewidth and spectral bandwidth of the original input optical pulse $g(t)$, respectively. Then, the signal at the output of the typical TPS system, $s\,(t)$, can be expressed as the convolution between the input optical signal and the Fourier transform of the intensity modulation function due to the real-time Fourier transform process in the typical TPS system [20]

$$\begin{aligned} s(t) &= g(t) * E_{\mathrm{IM}}(\omega)|_{\omega = t/\Delta\ddot{\Phi}_1} \\ &= S_0[g(t - \Delta t) + g(t + \Delta t)] \end{aligned} \tag{6}$$

where $E_{\mathrm{IM}}(\omega) = \Im[e_{\mathrm{IM}}(t)]$ is the Fourier transform of $e_{\mathrm{IM}}(t)$, (*) denotes the convolution operation, $S_0 = J_1(\beta)/|\ddot{\Phi}_1|$ is a time-independent constant, and $\Delta t = |\omega_m\ddot{\Phi}_1|$ is a time delay introduced by the balanced TPS process. According to (6), two replicas of the input optical pulse with a time delay difference of $2\Delta t$ are generated at the output of the typical TPS system that corresponds to the two first-order optical sidebands at the output of the MZM that is biased to suppress the carrier and the even-order sidebands.

Then, the complex electrical field of the optical pulse at the output of the entire UB-TPS system, $r(t)$, is obtained by propagating the signal $s(t)$ through the second subsystem that is simply the residual DE. The input and output signals are related by the temporal convolution $r(t) = s(t) * h_\Delta(t)$, where $h_\Delta(t) = \Im^{-1}[H_\Delta(\omega)]$ is the impulse response of the residual DE. If the dispersion of the residual DE satisfies the condition $|\Delta\ddot{\Phi}| \gg \tau_0^2/2\pi$, the spectra of the individual pulses ($g(t - \Delta t)$ and $g(t + \Delta t)$) are mapped to the time domain as two transformed waveforms ($\Im[g(t - \Delta t)]|_{\omega = t/\Delta\ddot{\Phi}}$ and $\Im[g(t + \Delta t)]|_{\omega = t/\Delta\ddot{\Phi}}$) due to the dispersion-induced real-time Fourier transform [16]. Since the two transformed waveforms

are time-delayed, the time delay difference Δt represents a corresponding frequency shear $\Delta\omega$ given by $\Delta\omega = \Delta t/\Delta\ddot{\Phi}$ based on the mapping relationship. Therefore, the two transformed waveforms can be expressed as

$$\Im[g(t-\Delta t)] = G(\omega-\Delta\omega)|_{\omega=t/\Delta\ddot{\Phi},\Delta\omega=\Delta t/\Delta\ddot{\Phi}} \quad (7a)$$

$$\Im[g(t+\Delta t)] = G(\omega+\Delta\omega)|_{\omega=t/\Delta\ddot{\Phi},\Delta\omega=\Delta t/\Delta\ddot{\Phi}} \quad (7b)$$

where $G(\omega) = \Im[g(t)] = |G(\omega)|\exp[j\Psi(\omega)]$ is the complex spectrum of the original input pulse $g(t)$, with $|G(\omega)|$ and $\Psi(\omega)$ being the spectral magnitude and phase terms, respectively, and $\Delta\omega$ is the corresponding frequency shear resulted from the time delay difference between the two time-delayed transformed waveforms [14]. Then, the output signal $r(t)$ from the entire UB-TPS system is given by

$$r(t) \propto [G(\omega+\Delta\omega)+G(\omega-\Delta\omega)]_{\omega=t/\Delta\ddot{\Phi},\Delta\omega=\Delta t/\Delta\ddot{\Phi}} \quad (8)$$

Note that the time-independent phase terms have been ignored in (8).

Finally, the two time-delayed and stretched optical pulses are sent to a high-speed PD. The electrical current at the output of PD is proportional to the intensity of the input electrical field that is given by

$$\begin{aligned} I(t) &\propto |r(t)|^2 \\ &= |G(\omega+\Delta\omega)|^2 + |G(\omega-\Delta\omega)|^2 \\ &\quad + 2|G(\omega+\Delta\omega)||G(\omega-\Delta\omega)| \\ &\quad \times \cos\,[2\Delta\omega t + \Delta\Psi(\omega)]_{\omega=t/\Delta\ddot{\Phi}} \end{aligned} \quad (9)$$

where $\Delta\Psi(\omega) = \Psi(\omega+\Delta\omega) - \Psi(\omega-\Delta\omega)$ is the relative phase difference between the two sheared spectral phases. From (9), we can see that the spectral interferometry is performed in the time domain, realized based on the linear frequency-to-time conversion given by $\omega = t/\Delta\ddot{\Phi}$.

Note that our proposed pulse characterization method has three major design parameters: the dispersion $\ddot{\Phi}_1$, the modulation frequency ω_m, and the residual dispersion $\Delta\ddot{\Phi}$. For the input optical pulse with a given bandwidth, the selection of $\ddot{\Phi}_1$ and ω_m is determined by (5). The bandwidth requirement for the modulation process can be reduced by choosing a greater value of $\ddot{\Phi}_1$. However, a greater value of $\ddot{\Phi}_1$ may also introduce unwanted TOD. On the other hand, the residual dispersion must be large enough such that $|\Delta\ddot{\Phi}| \gg \tau_0^2/2\pi$. In fact, a larger value of residual dispersion is always preferred to achieve more accurate frequency-to-time mapping that will improve the characterization accuracy, and to obtain a temporal interference pattern with a longer duration and lower frequency that will ease the bandwidth requirement for photodetection. In addition, the TOD introduced by the residual DE can be properly modeled in our analysis (see Section IV-A). Therefore, three design parameters are interlinked and need to be determined according to the specific requirements.

The proposed UB-TPS system is first investigated by numerical simulations. In the calculations, we assume that the sinusoidal microwave modulating signal has a frequency of $f_m = 4$ GHz. The phase modulation index β is 0.35 rad. The two DEs are a standard SMF and a dispersion compensating fiber (DCF). The dispersion values of the first and second DEs are selected to be $\ddot{\Phi}_1 = 435$ ps^2/rad and $\ddot{\Phi}_2 = -1260$ ps^2/rad, respectively. In the simulations, the PUT is a slightly dispersed optical pulse with an FWHM of 2.5 ps that is obtained by passing a transform-limited Gaussian optical pulse through a 60-m-long standard SMF. Fig. 2(a) and (b) shows the complex temporal profile and optical power spectrum of the input pulse, respectively. The input pulse is stretched by the first DE ($\ddot{\Phi}_1$), modulated by the sinusoidal microwave signal in the DSB-SC modulation scheme, and then, completely compressed by a complementary DE ($-\ddot{\Phi}_1$). The temporal signal at the output of the typical TPS system is shown in Fig. 2(c). Two short pulses that are the replicas of the input optical pulse and are separated by a time shift of $2\Delta t$ are observed, as predicted by (6). It can be seen that both the magnitude and phase of the original input optical pulse are maintained in the two replicas. The optical power spectrum of the two output pulses is shown in Fig. 2(d). A spectral interference is obtained due to the introduced time delay difference between the two pulses. Fig. 2(e) and (f) shows the temporal and spectral intensity profiles of the signal at the output of the entire UB-TPS system. By comparing the results shown in Fig. 2(d) and (e), we can see that spectral interferometry is performed in the time domain due to the real-time Fourier transform in the residual DE. An equivalent frequency shear is obtained by time shifting the Fourier-transformed waveforms.

Therefore, the proposed UB-TPS system is playing two roles, as an optical interferometer and a frequency-to-time mapper, both are critical for achieving a good performance for the optical pulse characterization system. Specifically, the first subsystem (the typical TPS system) generates two time-delayed replicas of the input optical pulse to be characterized, as indicated by (6), without using an optical interferometer implemented by using discrete components. The system stability is thus greatly improved. The time delay difference between the two pulse replicas can be accurately controlled and easily tuned by controlling the microwave modulation frequency. The second subsystem, which is simply the residual DE, is then employed to map the spectra of the two time-delayed optical pulses to two transformed waveforms with a corresponding frequency shear. The spectral interferometry is performed in the time domain, due to the real-time frequency-to-time mapping, as indicated by (9). Therefore, a stable temporal interference pattern is obtained for an individual input optical pulse that can be recorded by a high-speed oscilloscope in real time. The proposed technique enables single-shot pulse measurement based on the time-domain self-reference of the input pulse.

III. Pulse Characterization by the UB-TPS System

A. Pulse Characterization Procedure

The complete characterization of an ultrashort optical pulse can be performed based on temporal interferometry by using the proposed UB-TPS system. The optical pulse characterization procedure is illustrated in Fig. 3.

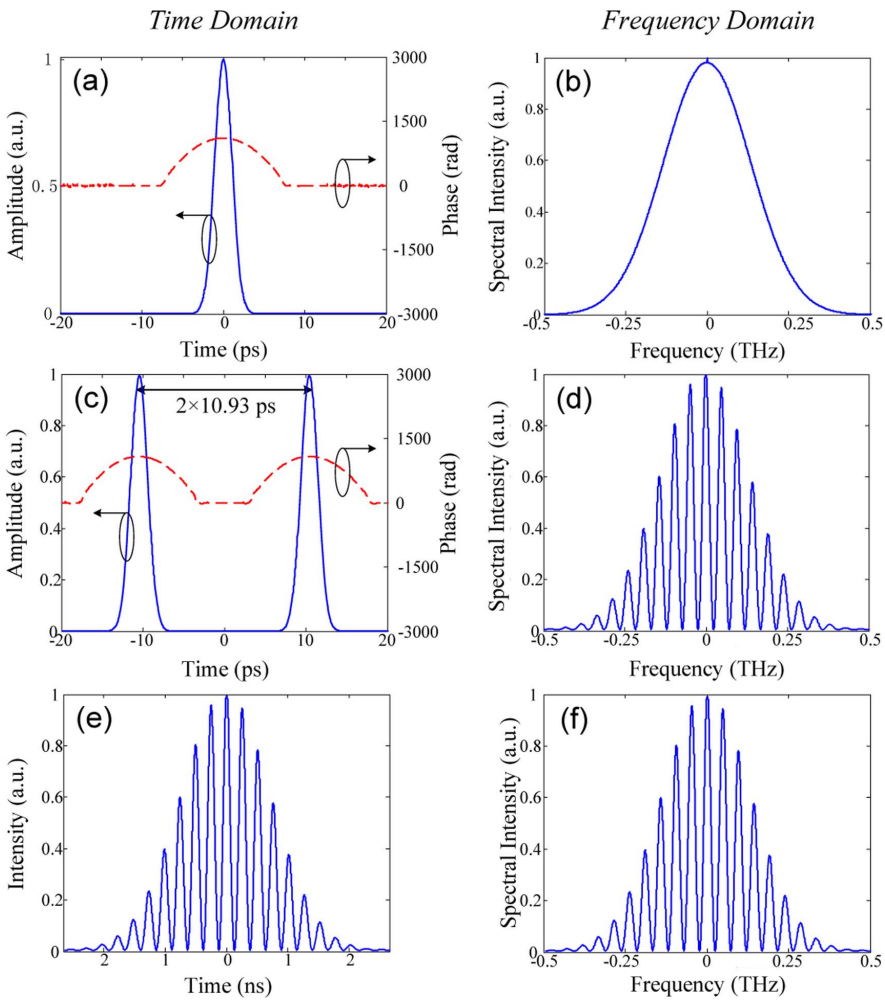

Fig. 2. Simulations performed to evaluate the UB-TPS system performance. (a) Complex temporal profile of the input optical pulse with the amplitude shown as solid line and phase shown as dashed line. (b) Optical power spectrum of the input pulse. (c) Complex temporal profile. (d) Optical power spectrum of the signal at the output of the typical TPS system. (e) Temporal intensity. (f) Optical power spectrum of the signal at the output of the entire UB-TPS system.

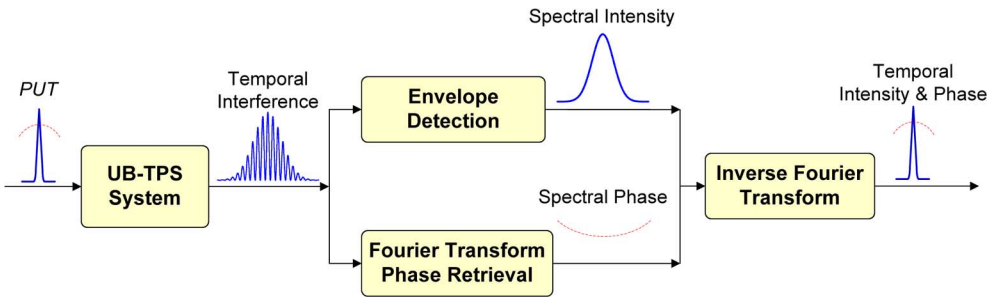

Fig. 3. Diagram showing the pulse characterization procedure based on temporal interferometry by using the proposed UB-TPS system. PUT: pulse under test and UB-TPS: unbalanced temporal pulse shaping.

The optical pulse to be characterized is sent to the UB-TPS system. A temporal interference pattern is obtained at the output of the UB-TPS system according to (9). If the frequency shear $\Delta\omega$ is small enough compared to the whole pulse bandwidth, i.e., $\leq$1% of the whole pulse bandwidth, we have $G(\omega+\Delta\omega)\approx G(\omega)$ and $G(\omega-\Delta\omega)\approx G(\omega)$, and (9) can be rewritten as

$$I(t)\propto 2|G(\omega)|^2\{1+\cos[2\Delta\omega t+\Delta\Psi(\omega)]\}_{\omega=t/\Delta\ddot{\Phi}} \quad (10)$$

where $|G(\omega)|^2$ is the spectral intensity of the input optical pulse. The phase difference can also be approximated as a differential expression $\Delta\Psi(\omega)\approx 2(d\Psi/d\omega)\Delta\omega$. From (10), we can see that $I(t)$ is a standard temporal interferogram that contains the information of both the spectral intensity of the original optical pulse and the relative spectral phase difference between the spectra of two frequency-sheared pulse replicas. The temporal interferogram consists of fringes with a nominal period of $T_n=\pi\Delta\ddot{\Phi}/\Delta t$ or a nominal frequency of $\omega_n=2\Delta\omega=$

$2\omega_m|\ddot{\Phi}_1/\Delta\ddot{\Phi}|$. If the input optical pulse is not transform-limited, the spectral phase difference $\Delta\Psi(\omega)$ would make the nominal fringe period nonconstant.

The spectral intensity $|G(\omega)|^2$ can be obtained by envelope detection of the recorded temporal interference pattern that can be done by extracting the baseband term using a Fourier transform technique. The spectral phase information is then retrieved by the well-known Fourier transform phase retrieval algorithm [22] that has been successfully employed for the measurement of chromatic dispersion [25]. First, the Fourier transform of the recorded temporal interference pattern is performed. To extract the spectral phase difference $\Delta\Psi(\omega)$ from the phase term in (10), the Fourier transform pattern is shifted by an amount of $2\Delta\omega$. One sideband will be shifted to the baseband (frequency downconversion), and the central band and the other sideband are no longer considered. By performing the Fourier transform of the shifted sideband, we obtain the phase term that gives directly the spectral phase difference $\Delta\Psi(\omega)$. Second, the spectral phase $\Psi(\omega)$ of the original optical pulse can then be obtained by either concatenating the spectral phase difference [10] or calculating the following integral [14]:

$$\Psi(\omega) = \frac{1}{2\Delta\omega}\int_{-\infty}^{+\infty}\Delta\Psi(\omega)d\omega. \tag{11}$$

Note that since the spectral interference is obtained from the temporal interference pattern, the frequency-to-time mapping relationship given by $\omega = t/\Delta\ddot{\Phi}$ must be applied to reconstruct the spectral intensity and phase. Finally, temporal intensity and phase of the original optical pulse can be obtained by calculating the inverse Fourier transform of the complex optical spectrum $G(\omega)$.

B. Experimental Results

The proposed optical pulse characterization approach is experimentally demonstrated based on the setup shown in Fig. 1. A passively mode-locked fiber laser (MLFL) is employed in our experiments as the optical source to generate a nearly transform-limited femtosecond Gaussian optical pulse train with a central wavelength of 1558 nm, a 3-dB spectral bandwidth of 8 nm (~1 THz), and a repetition rate of 48.6 MHz.

Two experiments are performed. In the first experiment, the complete characterization of a nearly transform-limited optical pulse is implemented. The ultrashort optical pulse from the MLFL is directly employed as the PUT and is characterized by using the proposed optical pulse characterization approach. As shown in Fig. 1, the PUT is first temporally stretched by the first DE that is a 2-km-long DCF with a dispersion of $\ddot{\Phi}_1 = 437.6$ ps^2/rad. Since the proposed technique is operating in the linear regime, the peak power of the input optical pulse is controlled low by using a tunable optical attenuator to avoid any nonlinear effects in the DCF. Considering the temporal width of an individual pulse is around 800 fs and the repetition rate of the pulse train is 48.6 MHz, the average power of the input optical pulse train is controlled to be lower than -18.8 dBm [23].

The stretched optical pulse is then modulated by a 4-GHz sinusoidal microwave signal at the MZM. The dispersion value and modulation frequency are selected to satisfy the condition given by (5). The DSB-SC modulation scheme is achieved by dc-biasing the MZM to operate at the minimum transmission point. The modulated optical pulse is then sent to the second DE that is a 60-km standard SMF with a dispersion of $\ddot{\Phi}_2 = -1261.2$ ps^2/rad. According to the discussion in Section II, the UB-TPS system here is equivalent to a typical balanced TPS system with two complementary DEs ($\ddot{\Phi}_1$ and $-\ddot{\Phi}_1$), followed by a residual DE with a dispersion of $\Delta\ddot{\Phi} = -823.6$ ps^2/rad. Therefore, two time-delayed replicas of the PUT are generated at the output of the balanced TPS system. The two replicas have an expected time delay difference of $2\Delta t = 22$ ps according to (6). The corresponding frequency difference is $2\Delta\omega = 4.25$ GHz (~0.4% of the whole bandwidth of the original pulse). The two time-delayed optical pulses are then stretched by the residual DE that has an adequate dispersion such that $|\Delta\ddot{\Phi}| \gg \tau_0^2/2\pi$ is satisfied. The temporal interference between the two time-delayed and dispersed pulses is detected by the PD and recorded by an oscilloscope, with the result shown in Fig. 4(a). Note that the proposed system enables single-shot pulse measurement. Although the input from the MLFL is a periodic optical pulse train in our case, the temporal interference pattern is measured by a real-time oscilloscope without performing any averaging. Fig. 4(b) shows the zoom-in view of the interference pattern inside the dashed box. The nominal period of the fringes is measured as 233.6 ps that matches very well with the expected value of 234.5 ps by (10).

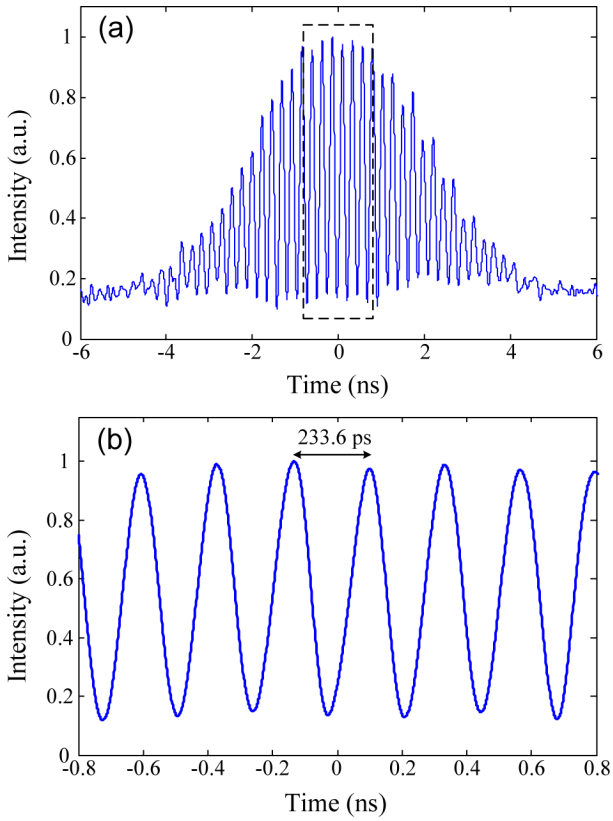

Fig. 4. (a) Measured temporal interference pattern between two time-delayed and stretched replicas of the PUT using a real-time oscilloscope. (b) Zoom-in view of the interference pattern in the dashed box in (a).

Although the interferometry is performed and measured in the time domain, the spectral interferometry can be directly

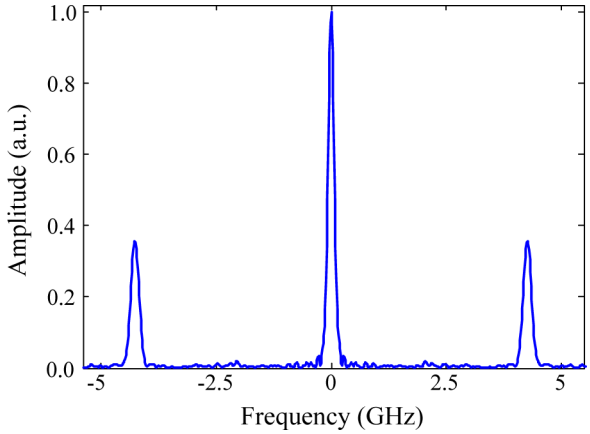

Fig. 5. Calculated Fourier transform (absolute value) of the interference pattern, as shown in Fig. 4(a).

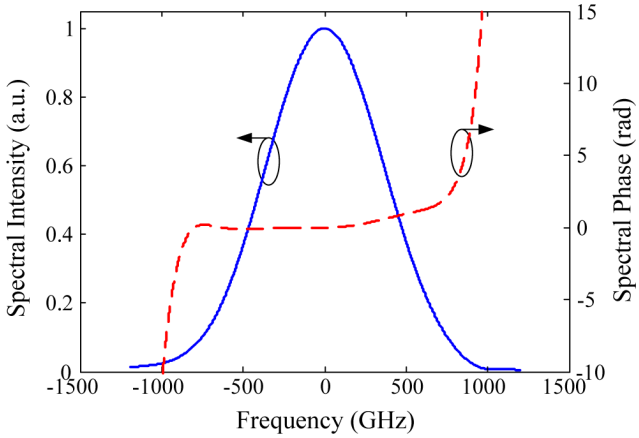

Fig. 6. Spectral intensity (solid line) and spectral phase (dashed line) of the PUT in the first experiment, reconstructed from the measured temporal interferogram.

obtained from the measured temporal interferogram due to the linear frequency-to-time mapping relationship given by $\omega = t/\Delta\ddot{\Phi}$. In reality, the frequency-to-time mapping process is not exactly linear due to the effect of higher order dispersion. This deviation has been taken into account in the calculations. The spectral interference trace is accurately obtained from the recorded temporal interference pattern according to the higher order dispersion-induced nonlinear frequency-to-time mapping [15]. This issue will be further discussed in more details in Section IV-A.

Fig. 5 shows the calculated Fourier transform (absolute value) of the interference pattern shown in Fig. 4(a). Two frequency sidebands located at ± 4.27 GHz are obtained, which matches well with the predicted nominal central frequency of 4.25 GHz given by (10). The central band contains the information of the interference pattern envelope. The absolute value of the inverse Fourier transform of the central band gives directly the spectral intensity $|G(\omega)|^2$. Then, the spectral phase information of the PUT is reconstructed from one of the sidebands following the Fourier transform phase retrieval procedure, as described in Section III-A, with the results shown in Fig. 6. The spectral intensity and phase are plotted as solid line and dashed line, respectively.

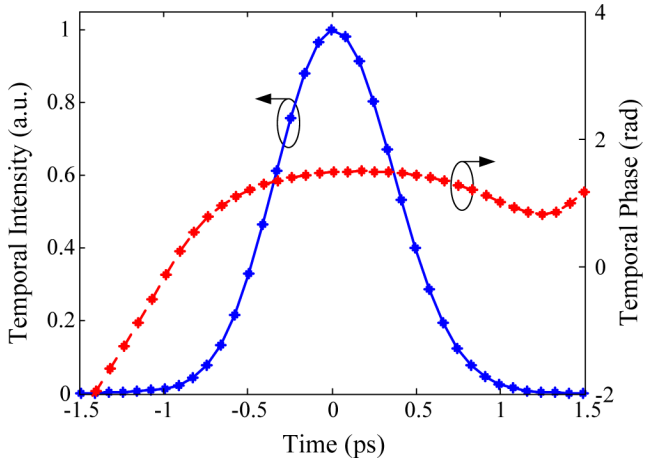

Fig. 7. Retrieved temporal intensity (solid line) and phase (dashed line) of the PUT in the first experiment, calculated from the inverse Fourier transform of Fig. 6.

By calculating the inverse Fourier transform of the complex pulse spectrum, as shown in Fig. 6, we finally obtain the temporal intensity and phase of the PUT, with the results shown in Fig. 7. The reconstructed optical pulse has a Gaussian shape temporal intensity profile with an FWHM of 810 fs. We also observe a small (0.7 rad) phase variation across the main pulse window. The time–bandwidth product (TBWP) of the reconstructed optical pulse is calculated to be 0.77 that is a little larger than the value of a transform-limited Gaussian pulse (0.44). The small pulse chirp is mainly resulted from the material dispersion and self-phase modulation in the MLFL.

In the second experiment, to further evaluate the proposed system, a slightly dispersed optical pulse is characterized. The original ultrashort optical pulse from the MLFL is sent through a 60-m-long standard SMF, and then, applied to the pulse characterization system as the PUT. It is known that the transmission of the transform-limited ultrashort optical pulse in the dispersive fiber would introduce some frequency chirping that would lead to the change of the phase profile. Fig. 8(a) and (b) shows the retrieved temporal intensity and phase profiles. The theoretically calculated profiles, obtained according to the spectral phase response of the 60-m-long standard SMF [23], are also shown for comparison. Fig. 8(c) shows the phase measurement errors between the measured and the calculated results. An average phase error as small as 0.6 rad is achieved within the main pulse window. The possible sources of the phase errors in our method include the inaccurate measurement of the dispersion (both the SOD and TOD), the slight nonlinear effects in the DEs, and the slightly inaccurate frequency-to-time mapping relationship (an approximation is always assumed [16]). The first error source can be eliminated by using a more accurate dispersion measurement method, such as the method proposed by Dorrer [25]. The nonlinear effects can be reduced by lowering the input optical power. The phase error caused by the approximated frequency-to-time mapping is intrinsic to the method, which, however, can be reduced by using greater residual dispersion.

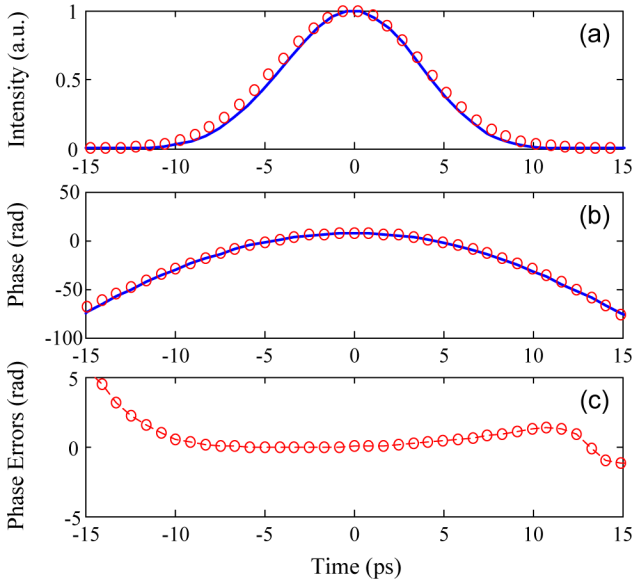

Fig. 8. Measured (circles) and calculated (solid line) (a) temporal pulse intensity profile and (b) temporal phase profile of the PUT in the second experiment. (c) Measurement errors of temporal phase by comparing the measured and calculated results.

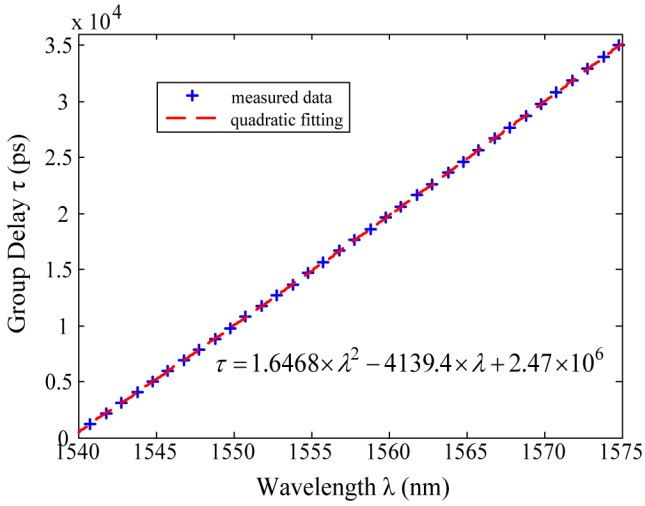

Fig. 9. Measured group delay response of the second DE by the conventional modulation phase shift method. Quadratic curve fitting result is also plotted as dashed line.

IV. Discussions

A. Effect of Higher Order Dispersion

In our analysis, the dispersion up to the second-order or the GVD ($\ddot{\Phi}$ in square picosecond per radian) was considered. For an ultrashort input optical pulse, the first DE with a moderate dispersion, i.e., a 2-km-long DCF in our experiments, is enough to temporally stretch the input pulse. Therefore, the TOD in the first DE is small and negligible. However, the dispersion in the second DE, i.e., a 60-km-long standard SMF in our experiments, is an adequate value to accomplish both the balanced TPS and the real-time Fourier transformation. Since the fiber is very long, the TOD ($\dddot{\Phi}$ in cubic picosecond per square radian) is large and has to be taken into account in the pulse characterization.

In this scenario, the second DE with both the GVD and TOD can be described by the following transfer function:

$$H_2(\omega) = H_{\mathrm{GVD}}(\omega) \times H_{\mathrm{TOD}}(\omega) \tag{12}$$

where $H_{\mathrm{GVD}}(\omega) = \exp(-j\ddot{\Phi}_2\omega^2/2)$ and $H_{\mathrm{TOD}}(\omega) = \exp(-j\dddot{\Phi}_2\omega^3/6)$. Recall that $\ddot{\Phi}_2 = -\ddot{\Phi}_1 + \Delta\ddot{\Phi}$; thus, the aforementioned transfer function can be rewritten as

$$H_2(\omega) = \exp\left(\frac{j\ddot{\Phi}_1\omega^2}{2}\right) \times \exp\left(-\frac{j\Delta\ddot{\Phi}\omega^2}{2}\right)\exp\left(-\frac{j\dddot{\Phi}_2\omega^3}{6}\right). \tag{13}$$

From (13), we can see that according to the property of a linear system, the second DE can be regarded as two cascaded subsystems. The first one, with only the GVD $(-\ddot{\Phi}_1)$, is employed as a complementary element to the first DE to perform the balanced TPS. The second subsystem, with both the GVD $(\Delta\ddot{\Phi})$ and the TOD $(\dddot{\Phi}_2)$, is functioning to stretch the two time-delayed pulses generated by the balanced TPS system and perform higher order dispersion-induced nonlinear frequency-to-time mapping [26]. As a result, even the input optical pulse is transform-limited, the temporal interference pattern would have a nonuniform period caused by the nonlinear mapping process. To precisely retrieve the spectral phase information, an accurate nonlinear frequency-to-time mapping relationship, taking into account both the GVD and the TOD, should be used. Based on [15], the nonlinear frequency-to-time mapping relationship is given by

$$\omega = \frac{t}{\ddot{\Phi}} - \frac{\dddot{\Phi}\,t^2}{2\ddot{\Phi}^3}. \tag{14}$$

By applying the aforementioned modified frequency-to-time mapping relationship, an accurate spectral interference pattern is obtained from the measured temporal interference pattern. To determine the GVD and TOD of the second DE (~60-km standard SMF), the group delay response of the SMF is measured in the range of 1545–1570 nm by the conventional modulation phase shift method [27], with the result shown in Fig. 9. The quadratic curve fitting of the experimental data is also plotted as dashed line. From the fitting result, we obtain the SOD and TOD as $\ddot{\Phi}_2 = 989.96$ ps/nm (or -1261.2 ps^2/rad) and $\dddot{\Phi}_2 = 3.29$ ps/nm^2 (or 5.34 ps^3/rad^2). These dispersion values are used in the nonlinear frequency-to-time mapping relationship given by (14).

B. Stability

It is worth noting that the accuracy of the spectral phase retrieved by the Fourier transform algorithm depends on the fringe visibility of the temporal interferogram. In the previous approaches, the backreflections [14] and poor alignment of the polarization states [15], [17] of the two interfering light beams in the interferometer would significantly degrade the fringe visibility of the interferogram. In addition, the optical interferometer is sensitive to environmental perturbations that will also lead to poor pulse characterization accuracy. In our proposed method, however, the two interfering signals are generated by the balanced TPS system incorporating the DSB-SC modulation and propagate through the same optical

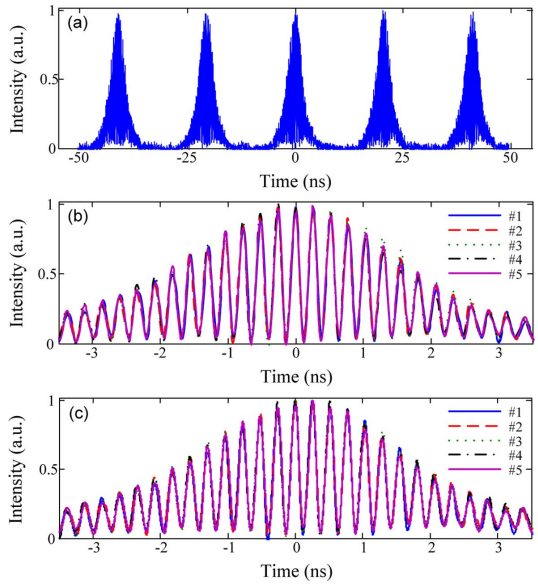

Fig. 10. Measured temporal interference patterns. (a) Five successive patterns. (b) Superimposed individual patterns of (a). (c) Interference patterns measured every 2 min in a 10 min period.

path that ensures that the two interfering signals always have an identical magnitude and maintain well-aligned polarization states. Therefore, a stable interferogram with a high fringe visibility can be achieved, leading to improved spectral phase measurement accuracy.

To investigate the system stability, more experimental measurements are performed. A stable periodic ultrashort optical pulse train with a repetition rate of 48.6 MHz from the MLFL is used as the input optical pulse in the measurements. The same experimental parameters and conditions as used in Section III-B are applied. The temporal interference patterns for five successive input optical pulses are measured by using a high-speed real-time oscilloscope, with the results shown in Fig. 10(a). For the purpose of comparison, the individual interference patterns are superimposed, as shown in Fig. 10(b). Five measurements are also performed for a period of 10 min with a 2 min interval. The measured interference patterns are shown in Fig. 10(c). We can see that the recorded temporal interference patterns are stable and maintain a good fringe visibility. Since the optical pulse train and the sinusoidal microwave modulation signal are not synchronized, slight fluctuations in the interference envelope are observed. For long-term operation, the bias drift of the MZM may become a critical issue that will affect the system stability that, however, can be resolved by using a simple bias stabilization circuit [28].

C. Reduced Processing Bandwidth

According to the analysis in Section II, the larger the dispersion in the first DE $\ddot{\Phi}_1$ and the higher the microwave modulation frequency f_m, the more the cycles will be contained in the generated temporal interference pattern, leading to a more accurate pulse characterization. On the other hand, the use of a DE with large dispersion may introduce high-order dispersion and the high-frequency microwave modulation may also increase the cost of the system; therefore, it is desirable to develop a guideline to choose the minimum number of cycles in the temporal interference pattern to ensure good measurement accuracy. In the following, a few more experimental measurements are performed to evaluate the impact of the number of cycles on the performance of the pulse characterization system. The PUT in the experiments is again the femtosecond optical pulse with an FWHM of 810 fs after propagating through a 60-m standard SMF. For the same system dispersion values of $\ddot{\Phi}_1 = 437.6$ ps^2/rad and $\ddot{\Phi}_2 = -1261.2$ ps^2/rad, the microwave modulation frequency is tuned at four different values of 5, 3, 0.85, and 0.65 GHz. The experimental results are shown in Fig. 11. The left column shows the measured temporal interference patterns. Different numbers of the cycles in the interference patterns are obtained. The right column shows the corresponding retrieved temporal phase profiles of the PUT. The calculated phase profiles according to the dispersion parameter of the 60-m-long standard SMF are also plotted as solid lines for comparison. Fig. 12 shows the root-mean-square error (RMSE) of the retrieved phase within the main pulse window, as a function of the number of cycles contained in the temporal interference patterns. It is clearly seen that the number of cycles must be greater than 10 to ensure good measurement accuracy.

In the proposed approach, the obtained temporal interference pattern with a nominal period of T_n is measured by a high-speed real-time oscilloscope. To perform a complete characterization of an input optical pulse, according to the sampling theorem, the sampling rate of the oscilloscope f_{osc} should satisfy the condition given by

$$f_{\text{osc}} > \frac{2}{T_n} = \frac{4 f_m \ddot{\Phi}_1}{\Delta\ddot{\Phi}}. \tag{15}$$

We can see that the required sampling rate is determined by the system dispersion and the microwave modulation frequency. The dispersion of the first DE $\ddot{\Phi}_1$ and the modulation frequency f_m must be properly selected to satisfy the condition in (5) and the dispersion of the residual DE $\Delta\ddot{\Phi}$ cannot be very large to avoid the higher order dispersion-induced interference pattern distortion, as discussed in Section IV-A. In our experiments, for the dispersion values ($\ddot{\Phi}_1 = 437.6$ ps^2/rad and $\Delta\ddot{\Phi} = -823.6$ ps^2/rad) and the modulation frequency ($f_m = 4$ GHz), the sampling rate of the oscilloscope should be higher than 8.5 GHz. In fact, by reducing the number of cycles in the interference pattern, a lower sampling rate is required while maintaining acceptable measurement accuracy. For example, when $f_m = 4$ GHz, the number of cycles is 32. By reducing the number to 10, the required microwave drive frequency is only 1.25 GHz that still satisfies the condition in (5). Clearly, a much lower sampling rate is needed. Therefore, the proposed method can find applications in the complete characterization of an ultrashort optical pulse, using relatively low-speed MZM, PD, and oscilloscope.

D. Adaptability

System adaptability is another key issue that should be taken into account for practical implementations. A good pulse characterization system should be able to measure optical pulses with a variety of pulse durations and phases. For example, the

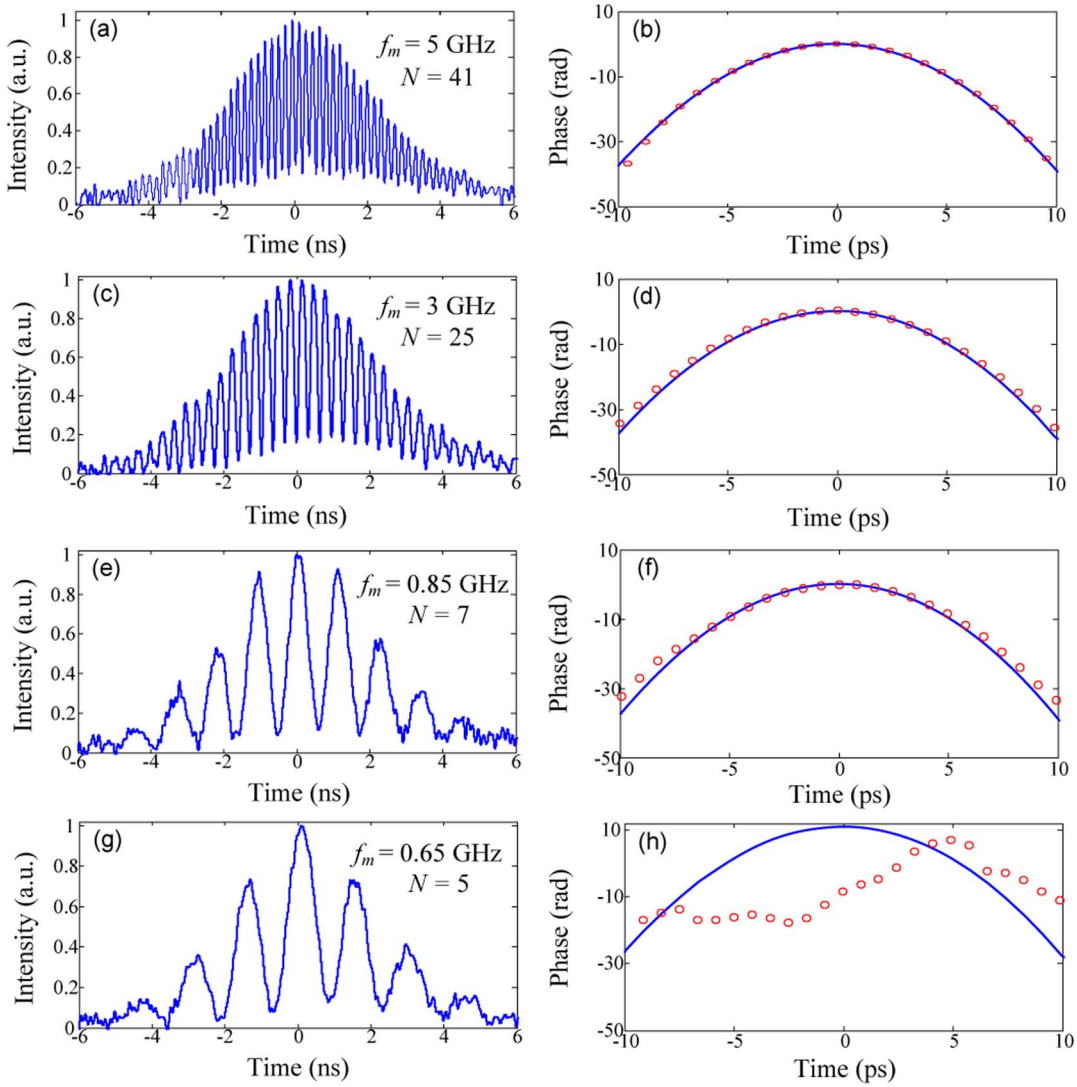

Fig. 11. Measured temporal interference patterns with four different modulation frequencies (left column) and the corresponding retrieved temporal phase profiles of the PUT (right column). (Solid line) Calculated temporal phase profiles.

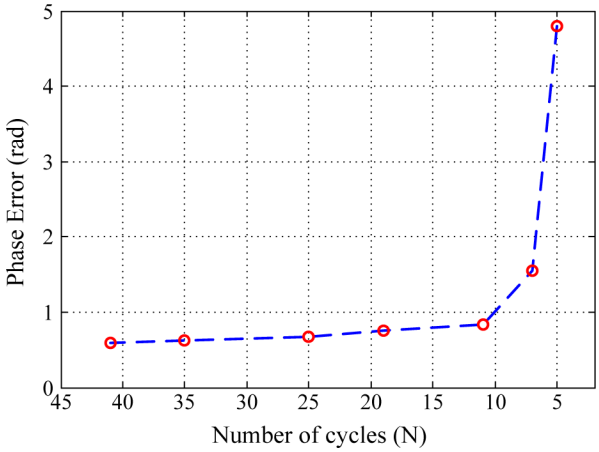

Fig. 12. RMSE of the phase measurement as a function of the number of cycles contained in the temporal interference pattern.

time delay difference between the two replicas of the original pulse should be tuned according to the pulse duration of the PUT to avoid pulse overlap. To show the importance of system adaptability, more simulations are carried out under the same simulation conditions as used in Section II. If the input optical pulse has a relatively large FWHM of 12 ps, at the output of the typical TPS system, the two pulse replicas are overlapped due to the small time delay, as shown in Fig. 13(a). Therefore, the time delay should be increased to avoid the significant measurement error due to the pulse overlap. Tuning the time delay was difficult in the previously reported systems where an optical interferometer based on a glass plate [14] or a fiber loop [15] was employed. In our proposed method, however, the time delay between the two pulse replicas can easily be tuned by controlling the microwave modulation frequency. As shown in Fig. 13(b), the two pulses are well-separated if the microwave modulation frequency is increased to 10 GHz. The original input pulse is also plotted as dashed line in Fig. 13. Therefore, the proposed technique works for characterization of both femtosecond and picosecond pulses.

Note that tuning the microwave modulation frequency may lead to the change of the nominal period of the temporal

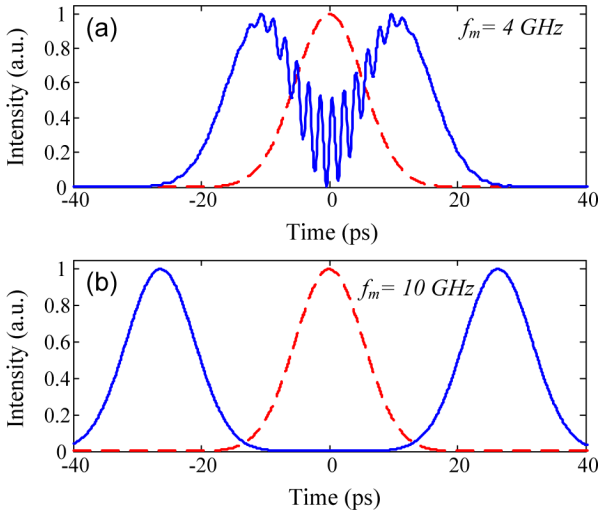

Fig. 13. Simulated signals at the output of the typical TPS system. (a) Microwave modulation frequency is 4 GHz. (b) Microwave modulation frequency is tuned to 10 GHz to increase the time delay between the two pulses. (Dashed line) Original input pulse.

interference pattern, as demonstrated in [21], where the proposed UB-TPS system was applied to achieve the microwave frequency multiplication. In fact, by properly controlling the dispersion values of the DEs [29], frequency division can also be realized. The significance of frequency division is that the temporal interference pattern may have a much lower carrier frequency than that of the microwave modulation signal; thus, a low-speed PD and oscilloscope are required, which would make the system less costly.

V. Conclusion

We have proposed and experimentally demonstrated a simple approach to achieving complete characterization of ultrashort optical pulse based on temporal interferometry in a UB-TPS system. The key innovation of this technique is that the system stability and tunability are significantly improved by replacing a fixed optical interferometer implemented, using discrete components in the previous techniques by an integrated MZM that was driven by a sinusoidal microwave modulation signal. In addition, the temporal interference pattern can be recorded in real time by a high-speed oscilloscope, making the system suitable for single-shot optical pulse characterization. The use of the proposed system for the complete characterization of an ultrashort optical pulse before and after passing through a 60-m standard SMF was experimentally demonstrated. The impact of high-order dispersion on the pulse characterization performance was also discussed. The use of lower microwave drive frequency to reduce the sampling rate, and eventually, to enable the use of relatively low-speed MZM, PD, and oscilloscope in the system was discussed. The stability and adaptability of the proposed system were also discussed.

References

[1] G. Steinmeyer, D. H. Sutter, L. Gallmann, N. Matuschek, and U. Keller, "Frontiers in ultrashort pulse generation: Pushing the limits in linear and nonlinear optics," *Science*, vol. 286, no. 10, pp. 1507–1512, Nov. 1999.

[2] C. Dorrer, "High-speed measurements for optical telecommunication systems," *IEEE J. Sel. Topics Quantum Electron.*, vol. 12, no. 4, pp. 843–858, Jul. 2006.

[3] K. Taira and K. Kikuchi, "Optical sampling system at 1.55 mm for the measurement of pulse waveform and phase employing sonogram characterization," *IEEE Photon. Technol. Lett.*, vol. 13, no. 5, pp. 505–507, May 2001.

[4] C. Dorrer and I. Kang, "Complete temporal characterization of short optical pulses using simplified chronocyclic tomography," *Opt. Lett.*, vol. 28, no. 16, pp. 1481–1483, Aug. 2003.

[5] C. Dorrer and I. Kang, "Real-time implementation of linear spectrograms for the characterization of high bit-rate optical pulse trains," *IEEE Photon. Technol. Lett.*, vol. 16, no. 3, pp. 858–860, Mar. 2004.

[6] I. A. Walmsley and C. Dorrer, "Characterization of ultrashort electromagnetic pulses," *Adv. Opt. Photon.*, vol. 1, no. 2, pp. 308–437, Apr. 2009.

[7] D. J. Kane and R. Trebino, "Characterization of arbitrary femtosecond pulses using frequency-resolved optical gating," *IEEE J. Quantum Electron.*, vol. 29, no. 2, pp. 571–579, Feb. 1993.

[8] R. G. M. P. Koumans and A. Yariv, "Time-resolved optical gating based on dispersive propagation: A new way to characterize optical pulses," *IEEE J. Quantum Electron.*, vol. 36, no. 2, pp. 137–144, Feb. 2000.

[9] C. Iaconis, V. Wong, and I. A. Walmsley, "Direct interferometric techniques for characterizing ultrashort optical pulses," *IEEE J. Sel. Topics Quantum Electron.*, vol. 4, no. 2, pp. 285–294, Apr. 1998.

[10] C. Iaconis and I. A. Walmsley, "Self-referencing spectral interferometry for measuring ultrashort optical pulses," *IEEE J. Quantum Electron.*, vol. 35, no. 4, pp. 501–509, Apr. 1999.

[11] V. Wong and I. A. Walmsley, "Analysis of ultrashort pulse-shape measurement using linear interferometers," *Opt. Lett.*, vol. 19, no. 4, pp. 287–289, Feb. 1994.

[12] R. M. Fortenberry, W. V. Sorin, H. Lin, S. A. Newton, J. K. Andersen, and M. N. Islam, "Low-power ultrashort optical pulse characterization using linear dispersion," in *Proc. Opt. Fiber Commun. Conf.*, 1997, pp. 290–291, Paper ThL3.

[13] F. Hakimi and H. Hakimi, "Measurement of optical fiber dispersion and dispersion slope using a pair of short optical pulses and Fourier transform property of dispersive medium," *Opt. Eng.*, vol. 40, no. 6, pp. 1053–1056, Jun. 2001.

[14] N. K. Berger, B. Levit, V. Smulakovsky, and B. Fischer, "Complete characterization of optical pulses by real-time spectral interferometry," *Appl. Opt.*, vol. 44, no. 36, pp. 7862–7866, Dec. 2005.

[15] H. Xia and J. P. Yao, "Characterization of subpicosecond pulses based on temporal interferometry with real-time tracking of higher order dispersion and optical time delay," *J. Lightwave Technol.*, vol. 27, no. 22, pp. 5029–5037, Nov. 2009.

[16] M. A. Muriel, J. Azaña, and A. Carballar, "Real-time Fourier transformer based on fiber gratings," *Opt. Lett.*, vol. 24, no. 1, pp. 1–3, Jan. 1999.

[17] T.-J. Ahn, Y. Park, and J. Azaña, "Pulse characterization using Hilbert transformation temporal interferometry (HTTI)," in *Proc. Conf. Lasers Electro-Opt./Quantum Electron. Laser Sci. Conf. Photon. Appl. Syst. Technol.*, 2007, pp. 1–2, OSA Tech. Dig. Series (CD) (Optical Soc. America), Paper JThD16..

[18] T.-J. Ahn, Y. Park, and J. Azaña, "Improved optical pulse characterization based on feedback-controlled Hilbert transformation temporal interferometry," *IEEE Photon. Technol. Lett.*, vol. 20, no. 7, pp. 475–477, Apr. 2008.

[19] C. Wang and J. P. Yao, "Complete pulse characterization based on temporal interferometry using an unbalanced temporal pulse shaping system," in *Proc. IEEE Int. Top. Microw. Photon. Meeting*, Oct. 2010, pp. 373–376, Paper FR1-4.

[20] H. Chi and J. P. Yao, "Symmetrical waveform generation based on temporal pulse shaping using amplitude-only modulator," *Electron. Lett.*, vol. 43, no. 7, pp. 415–417, Mar. 2007.

[21] C. Wang and J. P. Yao, "Continuously tunable photonic microwave frequency multiplication by use of an unbalanced temporal pulse shaping system," *IEEE Photon. Technol. Lett.*, vol. 22, no. 17, pp. 1285–1287, Sep. 2010.

[22] M. Takeda, H. Ina, and S. Kobayashi, "Fourier-transform method of fringe-pattern analysis for computer-based topography and interferometry," *J. Opt. Soc. Amer.*, vol. 72, no. 1, pp. 156–160, Jan. 1982.

[23] G. P. Agrawal, *Nonlinear Fiber Optics*, 2nd ed. New York: Academic, 1995.

[24] G. H. Qi, J. P. Yao, J. Seregelyi, S. Paquet, and C. Belisle, "Generation and distribution of a wideband continuously tunable millimeter-wave signal with an optical external modulation technique," *IEEE Trans. Microw. Theory Tech.*, vol. 53, no. 10, pp. 3090–3097, Oct. 2005.

[25] C. Dorrer, "Chromatic dispersion characterization by direct instantaneous frequency measurement," *Opt. Lett.*, vol. 29, no. 2, pp. 204–206, Jan. 2004.
[26] C. Wang and J. P. Yao, "Photonic generation of chirped millimeter-wave pulses based on nonlinear frequency-to-time mapping in a nonlinearly chirped fiber Bragg grating," *IEEE Trans. Microw. Theory Tech.*, vol. 56, no. 2, pp. 542–553, Feb. 2008.
[27] B. Costa, D. Mazzoni, M. Puleo, and E. Vezzoni, "Phase shift technique for the measurement of chromatic dispersion in optical fibers using LED's," *IEEE J. Quantum Electron.*, vol. QE-18, no. 10, pp. 1509–1515, Oct. 1982.
[28] J. Snoddy, Y. Li, F. Ravet, and X. Bao, "Stabilization of electro-optic modulator bias voltage drift using a lock-in amplifier and a proportional-integral-derivative controller in a distributed Brillouin sensor system," *Appl. Opt.*, vol. 46, no. 9, pp. 1482–1485, Mar. 2007.
[29] Y. Liu, J. Yang, and J. P. Yao, "Continuous true-time-delay beamforming for phased array antenna using a tunable chirped fiber grating delay line," *IEEE Photon. Technol. Lett.*, vol. 14, no. 8, pp. 1172–1174, Aug. 2002.

Chao Wang (S'08) received the B.Eng. degree in opto-electrical engineering from Tianjin University, Tianjin, China, in 2002, and the M.Sc. degree in optics from Nankai University, Tianjin, China, in 2005. He is currently working toward the Ph.D. degree in electrical and computer engineering at the University of Ottawa, Ottawa, ON, Canada.

His current research interests include all-optical microwave arbitrary waveform generation and processing, coherent optical pulse shaping, optical signal processing, radio-over-fiber systems, advanced fiber Bragg gratings, and their applications in microwave photonics systems.

Mr. Wang was the recipient of the SPIE Scholarship in Optical Science & Engineering (2008), the IEEE Photonics Society (formerly LEOS) Graduate Student Fellowship (2009), the Vanier Canada Graduate Scholarship (2009), the Chinese Government Award for Outstanding Self-Financed Students Abroad (2009), the IEEE MTT-S Graduate Fellowship (2010), and the Canada NSERC Postdoctoral Fellowship (2010). He is a Student Member of the IEEE Photonics Society, the IEEE Microwave Theory and Techniques Society, the Optical Society of America, and the International Society for Optical Engineering.

Jianping Yao (M'99–SM'01) received the Ph.D. degree in electrical engineering from the Université de Toulon, Toulon, France, in 1997.

From 1999 to 2001, he held a faculty position in the School of Electrical and Electronic Engineering, Nanyang Technological University, Singapore. In 2005, he was an Invited Professor in the Institut National Polytechnique de Grenoble, Grenoble, France. In 2007, he was appointed the University Research Chair in Microwave Photonics. In 2001, he joined the School of Information Technology and Engineering, University of Ottawa, Ottawa, ON, Canada, where he is currently a Professor, the Director of the Microwave Photonics Research Laboratory, and the Director of the Ottawa-Carleton Institute for Electrical and Computer Engineering. He has authored or coauthored over 300 papers, including over 170 papers in peer-reviewed journals and over 130 papers in conference proceedings. His current research interests include microwave photonics, all-optical microwave signal processing, photonic generation of microwave, millimeter wave and terahertz, radio over fiber, ultra wideband (UWB) over fiber, fiber Bragg gratings for microwave photonics applications, and optically controlled phased array antenna, as well as fiber lasers, fiber-optic sensors, and biophotonics. He is an Associate Editor of the *International Journal of Microwave and Optical Technology*. He is on the Editorial Board of the IEEE TRANSACTIONS ON MICROWAVE THEORY AND TECHNIQUES.

Dr. Yao was the recipient of the 2005 International Creative Research Award of the University of Ottawa, the 2007 George S. Glinski Award for Excellence in Research, and the NSERC Discovery Accelerator Supplements Award in 2008. He is a Registered Professional Engineer of the Province of Ontario. He is a Fellow of the Optical Society of America and a Senior Member of the IEEE Photonics Society and IEEE Microwave Theory and Techniques Society.